*Journal of Marine Research, 48,* 505–541, 1990

# Interaction between internal tides and energetic fluxes across the atmosphere-ocean interface over a continental shelf break

by R. Mazé[1] and J. Y. Le Tareau[1]

## ABSTRACT

Satellite infra-red images taken from April-May to September-October often show persistent ribbons of cool water along the European continental slope, from West Ireland to South-West Brittany (Pingree and Mardell, 1981; Le Tareau *et al.*, 1983; Mazé, 1983; Mazé *et al.*, 1986). The cooling increases northwestward and follows almost exactly the top of the shelf break. This effect appears to be connected with the increase in intensity of the baroclinic internal tide field. A global model is constructed to simulate the cooling process above the edge by interaction between internal tide waves and mixing. First, a three layer model simulates the generation and propagation of nonlinear waves induced over the shelf break as a result of the propagation of the barotropic tide. Then, mixing processes associated with wind action on the sea surface, tidal friction on the sea floor, and thermocline instability when the local Richardson number becomes less than $1/4$ are taken into account. Numerical runs on a transect perpendicular to the shelf break show the formation of a narrow spot of cool water above the edge when wind forcing is applied. This cool spot is advected by tidal currents from the slope to the shelf and conversely. Just above the shelf break, in the area of the internal tide generation, the internal mixing is larger than that taking place on the slope and on the shelf, leading to a thickening of the thermocline. On the other hand, a gust of wind has a very different effect on surface cooling during neap tides or spring tides. Thus, when the upper mixed layer is shallow, it appears that, during spring tides, a low intensity gust of wind is able to cool surface waters, whereas the same wind during neap tides induces no cooling.

Evidence of such characteristics have been observed in shelf break areas. In particular data collected during the *Ondine* 85 cruise in the Bay of Biscay show internal tides whose shape and amplitude can be compared with the model results. Shelf break cooling does not appear clearly in the temperature data. However, weak entrainment in the surface layer may be expected from nutrient data at spring tides (P. Le Corre, personal communication). The absence of a significant shelf break cooling can be explained by the presence of a rather deep seasonal thermocline (40 m depth in average) and weak winds during the experiment leading to low entrainment rates at spring tide on one hand, and by a positive heat budget for the ocean across the sea surface on the other hand. Therefore, a quasi-balance may be expected between cooling due to wind induced entrainment and warming due to a net surface heat flux positive in average over diurnal cycles during the experiment.

1. Laboratoire d'Oceánographie Physique, Faculté des Sciences, Av. Le Gorgeu, 29287 Brest Cedex, France.

## 1. Introduction

The aim of *Ondine* 85 cruise organized by the French Navy's Service Hydrographique et Océanographique de la Marine (SHOM) and the Physical Oceanography, Chemical Oceanography and Biological Oceanography Laboratories of the Université de Bretagne Occidentale during September, October and early November 1985, was to collect accurate field data to study internal waves in the northern part of the Bay of Biscay, and their action on spatial and temporal variations of different physical, chemical and biological parameters. On the other hand, theoretical work has been carried out to construct a numerical model to simulate generation and propagation of nonlinear internal waves induced over a shelf break by the barotropic tide wave. This model runs on a vertical transect perpendicular to the shelf break (Mazé, 1987). Another model, with the real topography of the Bay of Biscay, simulates generation and propagation of linear baroclinic tides over the whole area of the Bay of Biscay (Serpette and Mazé, 1990). In these two studies, the hypothesis of a two-layer ocean has been adopted. The results have been compared with the *Ondine* observations (Pichon and Mazé, 1990). The agreement between the predictions of the models and the measurements is qualitatively good. However, careful comparison shows that a more realistic vertical stratification of the ocean must be incorporated in the theoretical approach. Hereafter, a three-layer ocean model is considered: an upper well-mixed layer, a lower well-mixed layer, and between these two layers, a thermocline zone linearly stratified.

The purpose of the present work is to study, first theoretically, and then by means of observations, the importance of the interaction between wind mixing and internal tides upon the horizontal distribution of the physical properties of the sea. In this study, we consider a vertical transect perpendicular to a shelf break. The following variables are used: the depth of the upper boundary of the thermocline (thickness of the surface mixed layer), the depth of the lower boundary of the thermocline, the current components and the temperature in the upper and lower mixed layers.

## 2. Internal tide waves induced over a shelf break

The vertical ocean structure schematization and the notations used in the numerical model are shown in Figure 1. In the vertical direction the level of sea surface at rest is chosen as reference level.

*a. Hypothesis and notations.* In each layer the current is assumed to be the sum of a barotropic tidal component $\mathbf{U}$ and a baroclinic one $\mathbf{U}_i$ ($i = 1$ for the upper layer, $i = 2$ for the lower layer, $i = 3$ for the thermocline layer). The baroclinic currents $\mathbf{U}_1$ and $\mathbf{U}_2$ in the upper and in the lower mixed layer respectively are independent of the $z$ coordinate. In the intermediate thermocline layer a linear variation with respect to the vertical coordinate, of the baroclinic component $\mathbf{U}_3$, between $\mathbf{U}_2$ and $\mathbf{U}_1$ is assumed.

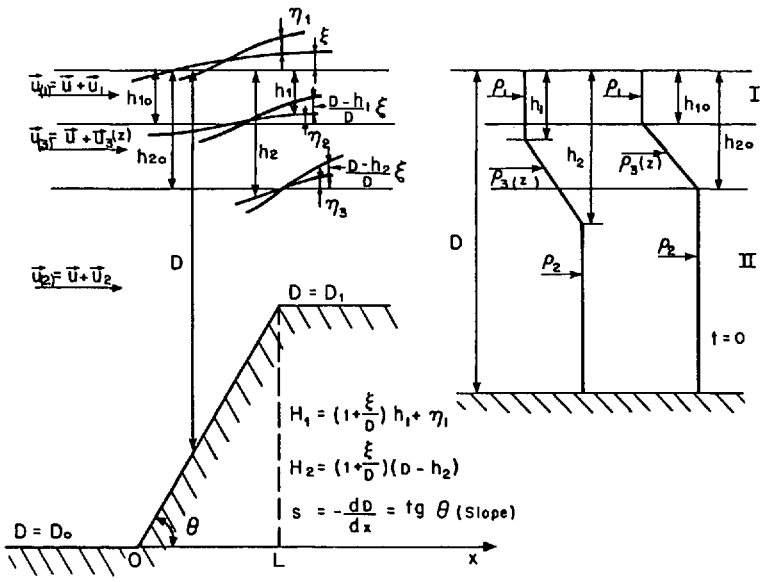


Figure 1. Diagrammatic representation and notations according to internal tide waves propagation in a three-layer ocean model.

The levels of the free surface and of the upper and lower boundary of the thermocline are also the sum of a barotropic tidal component and a baroclinic one. So the sea surface elevation is written: $\xi + \eta_1$.

$\xi$ is the elevation of the sea surface as the result of the tide in an homogeneous ocean, and $\eta_1$ is the departure from $\xi$ when the vertical structure is consistent with the three layer approximation.

As shown in Figure 1 the thickness of the upper mixed layer can be written:

$$H_1 = h_{1o} + \xi + \eta_1 - \xi_1 - \eta_2$$

with $\xi_1 = ((D - h_1)/D)\,\xi$; the thickness $h_1$ is defined as the position of the upper boundary of the thermocline with respect to the level of the free surface at rest in the presence of only the barotropic motion, $D$ is the water depth, $h_{1o}$ is the upper mixed layer thickness at rest, and $\eta_2$ is the baroclinic elevation of the upper boundary of the thermocline.

Thus we have:

$$H_1 = h_1 + \frac{h_1}{D}\xi + \eta_1 \simeq h_1\left(1 + \frac{\xi}{D}\right) \qquad \text{with} \qquad h_1 = h_{1o} - \eta_2.$$

In the same way, the thickness $h_2$ is defined as the position of the lower boundary of the thermocline with respect to its depth in the presence of the barotropic motion only.

Then the bottom layer thickness is:

$$H_2 = D - h_{2o} + \eta_3 + \frac{D - h_2}{D}\xi \qquad \text{with} \qquad h_2 = h_{2o} - \eta_3$$

Thus:

$$H_2 = (D - h_2)\left(1 + \frac{\xi}{D}\right)$$

In the expressions of $H_1$ and $H_2$, the terms $h_1/D\ \xi$ and $((D - h_2)/D)\ \xi$ serve to provide a reference for the variations in the level of the upper and lower boundary of the thermocline respectively, corresponding to the internal motion.

The variables which have to be determined are $h_1$ and $h_2$.

In the upper and lower mixed layers, densities are respectively $\rho_1$ and $\rho_2$. In the thermocline layer, the density $\rho_3(z)$ varies linearly with $z$, between $\rho_1$ and $\rho_2$.

The simplifying assumptions used in the model are represented in Figure 1. The $x$ axis is chosen positive in the on-shelf direction, perpendicular to the shelf break, which is assumed infinite along the direction $0y$. All the variables are therefore independent from $y$. The barotropic tide propagates along direction $0x$ and the shelf break has a constant slope $s$.

The barotropic motion is defined by the system of equations:

$$(A)\begin{cases}\dfrac{\partial \mathbf{U}}{\partial t} + (\mathbf{U} \cdot \overrightarrow{\text{grad}})\mathbf{U} + f\mathbf{z}_0 \wedge \mathbf{U} = -\, g\,\overrightarrow{\text{grad}}\,\xi \\ \dfrac{\partial \xi}{\partial t} = -\ \text{div}\,[(D + \xi)\,\mathbf{U}]\end{cases}$$

where $f$ is the inertial frequency and $\mathbf{z}_0$ the unit upward vertical vector.

Assuming that the nonlinear terms in system (A) can be neglected, and that the barotropic tide takes the form of a plane wave (of amplitude $\xi_0$ and pulsation $\omega$), which, coming from the ocean, is partially transmitted over the shelf and partially reflected toward the abyssal plain, then the solution $\xi$ and $\mathbf{U}$ are given (Mazé, 1983) by the following expressions:

$$\xi = \frac{2\xi_o}{1 + \sqrt{\dfrac{D_o}{D_1}}}\left[\sqrt{\frac{D_o}{D_1}}\cos K_o x \cos\left[\omega t + K\left[\sqrt{\frac{D_1}{D_o}}\,\text{Log}\,\frac{D_o}{D_1} - \Phi\right]\right]\right.$$

$$\left. + \sin K_o x \sin\left[\omega t + K\left[\sqrt{\frac{D_o}{D_1}} - \Phi\right]\right]\right.$$

over the abyssal plain,

$$\xi = \frac{2\xi_o}{1 + \sqrt{\dfrac{D_o}{D_1}}}\sqrt{\frac{D_o}{D_1}}\cos\left[\omega t + K\left[\sqrt{\frac{D_1}{D_o}}\,\text{Log}\,\frac{D}{D_1} - \Phi\right]\right]$$

over the continental slope,

$$\xi = \frac{2\xi_o}{1 + \sqrt{\frac{D_o}{D_1}}} \sqrt{\frac{D_o}{D_1}} \cos\left(\omega t - K_1(x - L) - K\Phi\right)$$

over the continental shelf.

with

$D_o$: water depth over the abyssal plain

$D_1$: water depth over the continental shelf

$K_o = \sqrt{\frac{\omega^2 - f^2}{gD_o}}$ : wave number over the abyssal plain

$K_1 = \sqrt{\frac{\omega^2 - f^2}{gD_1}}$ : wave number over the continental shelf

$K = \frac{K_o D_o}{s}$ : wave number over the continental slope

$s = -\frac{dD}{dx}$ : continental slope

$\Phi = \frac{\sqrt{D_o/D_1} + \mathrm{Log}\,(D_o/D_1)}{1 + \sqrt{D_o/D_1}}$

$L$: slope width

In the above expressions the origin of the $x$ coordinate is at the bottom of the continental slope.

The components of **U** are defined by:

$$U = \frac{g}{\omega^2 - f^2} \frac{\partial^2 \xi}{\partial x \partial t} \qquad \text{in the } 0x \text{ direction}$$

$$V = -\frac{gf}{\omega^2 - f^2} \frac{\partial \xi}{\partial x} \qquad \text{in the } 0y \text{ direction}$$

As an example, **U** over the continental shelf, is therefore given by the following expressions:

$$U = \frac{2\xi_o \omega}{K_o D\left(1 + \sqrt{\frac{D_o}{D_1}}\right)} \cos\left[\omega t + K\sqrt{\frac{D_1}{D_o}} \mathrm{Log}\,\frac{D}{D_1} - K\Phi\right]$$

$$V = \frac{2\xi_o f}{K_o D\left(1 + \sqrt{\frac{D_o}{D_1}}\right)} \sin\left[\omega t + K\sqrt{\frac{D_1}{D_o}} \mathrm{Log}\,\frac{D}{D_1} - K\Phi\right]$$

These expressions are introduced as forcing terms in the model of internal tides which is described below.

Such a barotropic forcing has already been used in previous two-layer models of baroclinic tides (Mazé *et al.*, 1986; Mazé, 1987).

*b. Model equations and closure assumption.* The fluid is assumed to be perfect; the system is therefore governed by Euler's equations on the one hand, and the continuity equations on the other hand.

Let $\mathbf{U}_{(i)}$ be the total current $\mathbf{U}_{(i)} = \mathbf{U}_i + \mathbf{U}$, $H_i$ the instantaneous thickness, $\rho_i$ the density and $P_i$ the pressure in the two well-mixed layers with $i = 1$ for the upper layer and $i = 2$ for the lower one.

The equations of motion and continuity are then:

$$\text{(B)} \begin{cases} \dfrac{\partial \mathbf{U}_{(i)}}{\partial t} + (\mathbf{U}_{(i)} \cdot \overrightarrow{\text{grad}})\, \mathbf{U}_{(i)} + f\mathbf{z}_0 \wedge \mathbf{U}_{(i)} = -\dfrac{1}{\rho_i} \overrightarrow{\text{grad}}\, P_i \\ \dfrac{\partial H_i}{\partial t} = -\ \text{div}\,(H_i \mathbf{U}_{(i)}) \end{cases}$$

Equations for the baroclinic motion are obtained by subtracting the system (A) from the system (B). In terms of position of upper and lower boundary of the thermocline $h_i$, and current components $(u_i, v_i)$, these equations can by written in the coordinate system defined in Section 2.a:

$$\text{(I)} \begin{cases} \dfrac{\partial h_1}{\partial t} = -\ UD \dfrac{\partial}{\partial x}\left(\dfrac{h_1}{D}\right) - \dfrac{1}{1 + \dfrac{\xi}{D}} \dfrac{\partial}{\partial x}\left[\left(1 + \dfrac{\xi}{D}\right) h_1 u_1\right] & \text{(I1)} \\ \dfrac{\partial u_1}{\partial t} + (U + u_1)\dfrac{\partial u_1}{\partial x} + u_1 \dfrac{\partial U}{\partial x} - fv_1 = -\dfrac{1}{\rho_1}\dfrac{\partial P_1}{\partial x} + g\dfrac{\partial \xi}{\partial x} & \text{(I2)} \\ \dfrac{\partial v_1}{\partial t} + (U + u_1)\dfrac{\partial v_1}{\partial x} + u_1 \dfrac{\partial V}{\partial x} + fu_1 = 0 & \text{(I3)} \\ \dfrac{\partial h_2}{\partial t} = -\ UD \dfrac{\partial}{\partial x}\left(\dfrac{h_2}{D}\right) - \dfrac{1}{1 + \dfrac{\xi}{D}} \left[\dfrac{\partial}{\partial x}\left[\left(1 + \dfrac{\xi}{D}\right) h_1 u_1\right] + \dfrac{\partial}{\partial x}\left[\left(1 + \dfrac{\xi}{D}\right)(h_2 - h_1)\dfrac{u_1 + u_2}{2}\right]\right] & \text{(I4)} \\ \dfrac{\partial u_2}{\partial t} + (U + u_2)\dfrac{\partial u_2}{\partial x} + u_2 \dfrac{\partial U}{\partial x} - fv_2 = -\dfrac{1}{\rho_2}\dfrac{\partial P_2}{\partial x} + g\dfrac{\partial \xi}{\partial x} & \text{(I5)} \\ \dfrac{\partial v_2}{\partial t} + (U + u_2)\dfrac{\partial v_2}{\partial x} + u_2 \dfrac{\partial V}{\partial x} + fu_2 = 0 & \text{(I6)} \end{cases}$$

The internal tide is described by equations (I1), (I2), (I3) in the upper mixed layer, and by Eqs. (I4), (I5), (I6) in the lower one.

In these equations, the variations with respect to the $y$ coordinate have been neglected. Thus the system of Eqs. (I) can only describe baroclinic motion and interface depths on a vertical transect perpendicular to the shelf break.

$U$ and $V$ which are the components of the barotropic tidal current, are given by analytical expressions (see Section 2.a).

The pressure gradient terms must be specified:

$$-\frac{1}{\rho_1}\frac{\partial p_1}{\partial x} = -g\frac{\partial}{\partial x}(\eta_1 + \xi)$$

$$-\frac{1}{\rho_2}\frac{\partial p_2}{\partial x} = -g\frac{\rho_1}{\rho_2}\frac{\partial(\eta_1 + \xi)}{\partial x} + g'\frac{\partial}{\partial x}\left[\left(\frac{h_1 + h_2}{2}\right)\left(1 + \frac{\xi}{D}\right)\right]$$

if hydrostatic pressure is assumed and $g' = g\,\delta\rho/\rho_z$ is the reduced gravity ($\delta\rho = \rho_2 - \rho_1$).

In the pressure gradient terms and in the continuity equations (I1) and (I4), the term $\xi/D$ can be neglected ($\xi/D \ll 1$).

In order to close the system of Eqs. (I), an assumption must be made with respect to the relationship between the variation in the level of the free surface and the thermocline. In the linear problem, a relation between $\eta_1$, $h_1$ and $h_2$ can be easily derived. Thus, neglecting the nonlinear terms in the equations of motion and assuming that the motion over the continental slope is associated with a simple sine wave function of time, then, in the absence of a barotropic tide, the motion in the two mixed layers, and the position of the thermocline are described by the following equations:

$$j\omega u_1 - fv_1 = -g\frac{\partial \eta_1}{\partial x}$$

$$j\omega v_1 + fu_1 = 0$$

$$j\omega u_2 - fv_2 = -g\frac{\partial \eta_1}{\partial x} + g'\frac{\partial}{\partial x}\left(\eta_1 + \frac{h_1 + h_2}{2}\right)$$

$$j\omega v_2 + fu_2 = 0$$

$$\frac{\partial}{\partial t}(\eta_1 + h_2) = -\frac{\partial}{\partial x}\left[(h_1 + \eta_1)u_1 + (h_2 - h_1)\frac{u_1 + u_2}{2}\right]$$

$$\frac{\partial h_2}{\partial t} = \frac{\partial}{\partial x}[(D - h_2)\,u_2]$$

with $j = \sqrt{-1}$

Eliminating $u_1$, $v_1$, $u_2$ and $v_2$ and writing $\partial\eta_1/\partial t = j\,\omega\,\eta_1$ gives:

$$\eta_1 = -\frac{g}{\omega^2 - f^2} \cdot \frac{\partial}{\partial x}\left[D\left(1 + \frac{\eta_1}{D} - \frac{g'}{g}\left(1 - \frac{h_1 + h_2}{2D}\right)\right)\frac{\partial \eta_1}{\partial x} - \frac{g'}{g}\left(D - \frac{h_1 + h_2}{2}\right)\frac{\partial}{\partial x}\left(\frac{h_1 + h_2}{2}\right)\right]$$

With the approximations:

$$\frac{\eta_1}{D} \ll 1 \qquad \text{and} \qquad \frac{g'}{g}\left(1 - \frac{h_1 + h_2}{2D}\right) \ll 1,$$

this expression becomes:

$$\eta_1 = -\frac{g}{\omega^2 - f^2}\frac{\partial}{\partial x}\left[D\frac{\partial \eta_1}{\partial x} - \frac{g'}{g}\left(D - \frac{h_1 + h_2}{2}\right)\frac{\partial}{\partial x}\left(\frac{h_1 + h_2}{2}\right)\right]$$

The order of magnitude of the first term on the right-hand can be estimated and compared to $\eta_1$.

This gives the ratio $g\,k^2\,D/(\omega^2 - f^2)$, where $k$ is the wavenumber of the internal tide.

In the Bay of Biscay this ratio is of the order $10^4$ ($\omega = 1.4\ 10^{-4}\,s^{-1}$, $f = 1.0\ 10^{-4}\,s^{-1}$, $D = 200$ m, $k = 2.1\ 10^{-4}\,m^{-1}$ for an internal tide of wavelength $\lambda = 30$ km).

In the above equation, $\eta_1$ can therefore be neglected on the left-hand side. According to this approximation, we can integrate this equation with respect to $x$:

$$D\frac{\partial \eta_1}{\partial x} - \frac{g'}{g}\left(D - \frac{h_1 + h_2}{2}\right)\frac{\partial}{\partial x}\left(\frac{h_1 + h_2}{2}\right) = F(t)$$

where $F$ is a function of time only. Over a flat bottom $F = 0$. Continuity at the limits of a continental slope implies that the same is true also over the slope, hence:

$$\frac{\partial \eta_1}{\partial x} \simeq \frac{g'}{g}\left(1 - \frac{h_1 + h_2}{2D}\right)\frac{\partial}{\partial x}\left(\frac{h_1 + h_2}{2}\right)$$

This approximation gives the relation between the baroclinic elevation of the sea surface and the instantaneous depth of the middle of the thermocline layer in the linear problem. This relationship will also be chosen as the closure assumption in our nonlinear model.

Such a hypothesis has already been used in a two-layer nonlinear model of internal tides. The results obtained in this case corroborated its validity (Mazé, 1987).

The pressure gradient terms, in Eqs. (I2) and (I5) become henceforth:

$$-\frac{1}{\rho_1}\frac{\partial P_1}{\partial x} + g\frac{\partial \xi}{\partial x} = -g'\left(1 - \frac{h_1 + h_2}{2D}\right)\frac{\partial}{\partial x}\left(\frac{h_1 + h_2}{2}\right)$$

$$-\frac{1}{\rho_2}\frac{\partial P_2}{\partial x} + g\frac{\partial \xi}{\partial x} = g'\frac{h_1 + h_2}{2D}\frac{\partial}{\partial x}\left(\frac{h_1 + h_2}{2}\right)$$

after neglecting terms of little importance in the last expression.

This hydrostatic balance is the closure hypothesis for system (I).

With these relations for the pressure gradient terms, and neglecting $\xi/D$ with respect to 1, the system of equations (I) becomes:

$$
(\mathrm{II})\begin{cases}
\dfrac{\partial h_1}{\partial t} = -UD\dfrac{\partial}{\partial x}\left(\dfrac{h_1}{D}\right) - \dfrac{\partial}{\partial x}(h_1u_1) & \text{(II1)}\\[2ex]
\dfrac{\partial u_1}{\partial t} + (U+u_1)\dfrac{\partial u_1}{\partial x} + u_1\dfrac{\partial U}{\partial x} - fv_1 = -g'\left(1 - \dfrac{h_1+h_2}{2D}\right)\dfrac{\partial}{\partial x}\left(\dfrac{h_1+h_2}{2}\right) & \text{(II2)}\\[2ex]
\dfrac{\partial v_1}{\partial t} + (U+u_1)\dfrac{\partial v_1}{\partial x} + u_1\dfrac{\partial V}{\partial x} + fu_1 = 0 & \text{(II3)}\\[2ex]
\dfrac{\partial h_2}{\partial t} = -UD\dfrac{\partial}{\partial x}\left(\dfrac{h_2}{D}\right) - \dfrac{\partial}{\partial x}(h_1u_1) + \dfrac{\partial}{\partial x}\left[(h_2-h_1)\dfrac{u_1+u_2}{2}\right] & \text{(II4)}\\[2ex]
\dfrac{\partial u_2}{\partial t} + (U+u_2)\dfrac{\partial u_2}{\partial x} + u_2\dfrac{\partial U}{\partial x} - fv_2 = g'\dfrac{h_1+h_2}{2D}\dfrac{\partial}{\partial x}\left(\dfrac{h_1+h_2}{2}\right) & \text{(II5)}\\[2ex]
\dfrac{\partial v_2}{\partial t} + (U+u_2)\dfrac{\partial v_2}{\partial x} + u_2\dfrac{\partial V}{\partial x} + fu_2 = 0 & \text{(II6)}
\end{cases}
$$

Eqs. (II1), (II2), (II3) are related to the upper mixed layer, (II4), (II5), (II6) to the lower one.

In these equations, the barotropic motion is prescribed according to the analytical expressions defined in Section 2.a.

The following limitations of the model must be emphasized:

— only the first baroclinic mode is retained;

— by assuming independency in the alongshelf direction topographic Rossby waves are also excluded;

— the barotropic tidal field is not modified by the baroclinic one.

*c. Numerical scheme, filtering process and boundary conditions.* The system of equations (II) is solved numerically using a leapfrog scheme for approximation of time derivatives, and centered finite difference quotients at the two nearest points for approximation of space derivatives.

At a given time $t$, the variables are defined on the $x$ axis as follows:

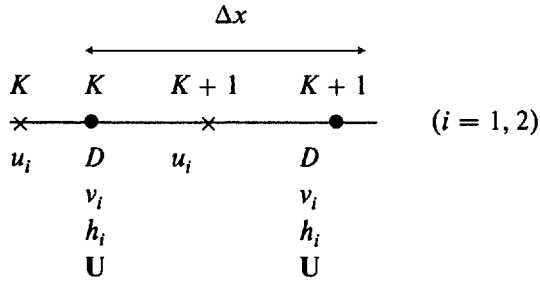


$(i = 1, 2)$

$\Delta x$ is the space increment on the transect, and $K$ denotes the distance from the origin in space increments, that is $x = K\Delta x$. In the same way, we have $t = N\Delta t$, where $\Delta t$ is the time increment.

For instance, the continuity equation (II1) is approximated by:

$$h_1(K, N+1) = h_1(K, N-1) - A - B$$

with:

$$A = U(K, N)D(K)[h_1(K+1, N)/D(K+1) - h_1(K-1, N)/D(K-1)](\Delta t/\Delta x)$$

$$B = [[h_1(K+1, N) + h_1(K, N)]u_1(K+1, N) - [h_1(K, N) + h_1(K-1, N)]u_1(K, N)](\Delta t/\Delta x)$$

In the same way, the equation (II2) is approximated by:

$$u_1(K, N+1) = u_1(K, N-1) - A' - B' + C' - D'$$

with:

$$A' = [\overline{U} + u_1(K, N)][u_1(K+1, N) - u_1(K-1, N)](\Delta t/\Delta x)$$

$$B' = 2\,u_1(K, N)[U(K, N) - U(K-1, N)](\Delta t/\Delta x)$$

$$C' = f(v_1(K, N) + v_1(K-1, N)]\Delta t$$

$$D' = g'[1 - (\overline{h}_1 + \overline{h}_2)/(2\overline{D})][h_1(K, N) + h_2(K, N) - h_1(K-1, N) - h_2(K-1, N)](\Delta t/\Delta x)$$

and:

$$\overline{U} = [U(K, N) + U(K-1, N)]/2$$

$$\overline{h}_i = [h_i(K, N) + h_i(K-1, N)]/2 \qquad (i = 1 \text{ or } 2)$$

$$\overline{D} = [D(K) + D(K-1)]/2$$

The same differencing procedure is applied to approximate the other equations of system (II).

The numerical values of the time increment $\Delta t$ and of the grid scale $\Delta x$ must be chosen in order to satisfy the stability criterion $\Delta x/\Delta t > C_m$, where $C_m$ is the maximal value for the celerity of propagation of induced motions. These are, in the present case, long internal tides that propagate nonlinearly in a moving medium. It is therefore difficult to set *a priori* a value for $C_m$, but an upper limit can be estimated as by the

condition:

$$C_m < \sqrt{g' \frac{\bar{h}\,(D - \bar{h})}{D}} \Big/ \left(1 - \frac{f^2}{\omega^2}\right) + |U| = C_1$$

where $\bar{h} = (h_1 + h_2)/2$ and $|U|$ is the amplitude of the barotropic current. With the numerical values actually used, $C_1$ will always be less than 1.5 m · $s^{-1}$.

Taking $\Delta x = 500$ m to have a good space accuracy over the slope, the numerical value of $\Delta t$ is accordingly chosen as $\Delta t = 120$ s.

With the leapfrog scheme and centered space differencing, spurious short-wave-noise appears both in space and time. These computational modes have to be suppressed in some way, otherwise they lead to a breakdown of the integration. The method used here to damp high frequency noise is time and space filtering.

Time filtering is applied at each time step and space filtering every three time steps to all the variables of system (II). Centered filters are used in both time and space. Let $X$ be one of these variables.

Time filtering is applied according to the relation:

$$\bar{X}(x, t) = X(x, t) + \tfrac{1}{2} S_t[\bar{X}(x, t - \Delta t) - 2X(x, t) + X(x, t + \Delta t)]$$

which is the Asselin time filter (Mesinger and Arakawa, 1976); $S_t$ is the filter parameter taken here as $S_t = 0.15$, and the overbar denotes the filtered value of $X$.

A three points filter is applied for space filtering:

$$\bar{X}(x, t) = X(x, t) + \tfrac{1}{2} S_x [X(x + \Delta x, t) - 2X(x, t) + X(x - \Delta x, t)] \qquad \text{with } S_x = 0.25$$

This filtering method in conjunction with the leapfrog scheme and space centered differencing gives, for the resolution of system (II), a procedure damping the high frequencies in a very selective way. With the numerical values chosen for $S_t$ and $S_x$, only a small amount of dissipation is introduced in the model and the associated reduction of the long internal tide amplitude is weak.

The initial conditions are taken as follows:

$$\begin{aligned} h_i(x, 0) &= h_i(x, -\Delta t) = h_{io} \\ u_i(x, 0) = v_i(x, 0) &= u_i(x, -\Delta t) = v_i(x, -\Delta t) = 0 \end{aligned} \qquad (i = 1 \text{ or } 2)$$

These initial conditions are incompatible with system (II), because they imply that the driving terms (forcing) are null at the initial time. To overcome this difficulty and to avoid spurious numerical waves of large amplitude which can appear as a result of the input initial conditions, the amplitude of the barotropic tide $\xi_o$, is replaced over the first tidal period by a function whose value is null at time t = 0 and which tends rapidly

toward a constant:

$$\xi_o (1 - e^{-t/\tau}) \qquad \text{with } \tau = 3 \text{ hrs}$$

Values of all variables, at the open boundaries on both ends of the domain, are determined by applying Orlanski's implicit condition (Orlanski, 1976).

Numerical experiments have been carried out over a transect of 400 km length, the shelf break being in the middle of the domain.

Initial values of all the variables were chosen as uniform along the $x$ axis.

Numerical runs have been carried out on an IBM 9370 Computer. A computer time of 250 seconds is needed for the simulation of a $M_2$ tidal period.

## 3. Mixing processes and vertical fluxes

*a. Description of mixing processes.* Under adiabatic conditions (no heat flux at the sea surface) and if mixing is not taken into account in the model, the reduced gravity $g'$ remains constant both in time and in space. Resolving the system of equations (II) gives then the baroclinic wave field on a vertical transect perpendicular to the shelf break, in a three layers medium where the upper and lower densities are not allowed to vary; thus vertical fluxes of mass, heat and momentum from one layer to another cannot occur.

If mixing processes are introduced in the model, the two mixed layers temperatures will vary. These bulk temperatures must then be defined in the whole domain, in order to calculate the reduced gravity $g'$ which appears in the pressure gradient terms of system (II).

A simple linear equation of state of sea water is assumed; salinity variations over the whole domain are ignored.

Let $T_i$ and $\rho_i = \rho_o [1 - \alpha_T (T_i - T_o)]$ be respectively the temperature and the density, of the upper mixed layer ($i = 1$) or of the lower mixed layer ($i = 2$).

Hence:

$$g' = g \frac{\rho_2 - \rho_1}{\rho_o} = g \alpha_T (T_1 - T_2)$$

where:

$\rho_o$ : reference density
$T_o$ : reference temperature
$\alpha_T$ : thermal expansion coefficient

Mixing induces space and time variations of bulk temperature in the two mixed layers. This leads to an interaction with the baroclinic wave field through variations of $g'$.

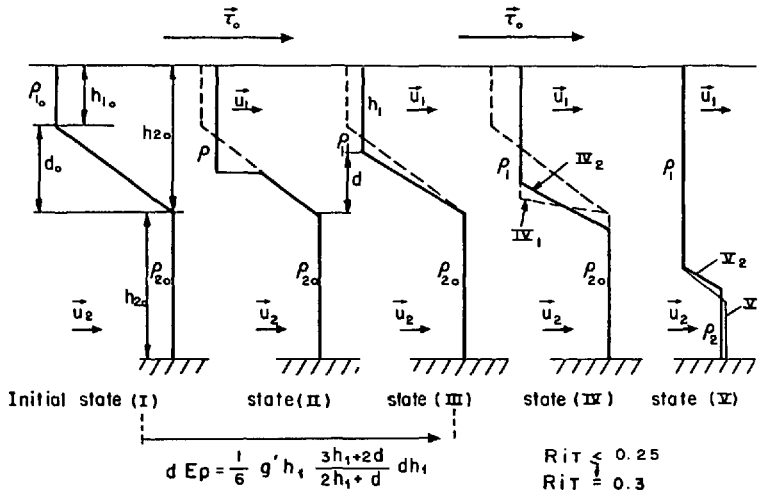


Figure 2. Vertical density structure variations according to mixing. I → II → III Surface effect mixing (wind stress on sea surface) $IV_1 \rightarrow IV_2$ Internal effect mixing (thermocline instabilities) $V_1 \rightarrow V_2$ Bottom effect mixing (tidal current stress on the sea floor).

The variations of temperature in the mixed layers are governed by the heat conservation equations given in Section 3.b (equations (X) and (XI)) and by the vertical mixing processes.

Three vertical mixing mechanisms are defined as follows:

— thermocline erosion in the upper part of the thermocline due to the Reynolds stress induced by the wind stress action on the sea surface; this process is called hereafter "surface effect mixing";

— mixing in the thermocline due to Kelvin-Helmholtz instabilities when the local Richardson number falls under ¼ (Thorpe, 1971; Sherman *et al.*, 1978; Turner, 1981); this process which occurs when the thermocline is narrow and the current shear large, is called hereafter "internal mixing";

— thermocline erosion in the lower part of the thermocline induced by shear generated by the tidal friction over the ocean bottom; this effect tends to widen the bottom mixed layer over the continental shelf and edge; its importance is relatively weak over the shelf slope where the lower layer thickness is large; this process is called hereafter "bottom effect mixing."

*i. Surface effect mixing*

Let $t_o$ be the time at which the wind begins to blow. Mixing will occur at time $t_1 > t_o$. At time $t_1$, and at any point on the transect, the water column structure is represented by state (I) (Fig. 2). Current velocities in the upper and lower mixed layers are respectively $U_{(1)} = U + U_1 + U_w$, $U_{(2)} = U + U_2$, i.e. the sum of a barotropic current

$\mathbf{U}$, a baroclinic component $\mathbf{U}_i$, and a vertically averaged wind induced current $\mathbf{U}_w$ (in the upper layer only). The densities in the upper and lower homogeneous layers are respectively $\rho_1$ and $\rho_2$, and $N$, the Brunt-Väisälä frequency in the thermocline layer is defined here by:

$$N^2 = g \frac{\rho_2 - \rho_1}{\rho_2 d}$$

where $g$ is the gravitational acceleration and $d$ the thermocline thickness. Because of wind mixing, erosion of the upper boundary of the thermocline appears, giving a density discontinuity represented by the vertical density structure (II). This discontinuity is not stable, and is only an intermediate state. It is assumed that some internal mixing process gives the vertical structure (III) as the result of wind action.

To get the vertical structure (III) from the initial one (I), an entrainment velocity parameterization $W_{e_1} = dh_1/dt$ is derived from the following expressions of the rate of potential energy variation of a water column:

$$\frac{dE\rho}{dt} = \alpha \rho_2 \frac{A_{v1}}{h_1} \mathbf{U}_w^2 - \frac{1}{2} \rho_2 \mathbf{u}_{-h}^2 \frac{dh_1}{dt} \qquad \text{(III)}$$

$$\frac{dE\rho}{dt} = \frac{1}{6} g (\rho_2 - \rho_1) h_1 \frac{3h_1 + 2d}{2h_1 + d} \frac{dh_1}{dt} \qquad \text{(IV)}$$

Where:

$\alpha$ : Dimensionless entrainment parameter

$\mathbf{u}_{-h}$ : Actual wind induced current at the bottom of the upper mixed layer

$h_1$ : Instantaneous upper mixed layer thickness

$d$ : Instantaneous thermocline thickness

$A_{v1}$ : Vertical eddy viscosity coefficient defined by $A_{v1} = v_{*1}^2/N\sqrt{2}$where $v_{*1}$ is the surface friction velocity given by $v_{*1} = \sqrt{\tau_s/\rho_1}$ and $\tau_s$ the surface wind stress

$\mathbf{U}_w = \mathbf{D}_w/h_1$ : Wind induced horizontal bulk velocity

$\mathbf{D}_w$ : Integrated horizontal momentum flux due to the wind

Eq. (III) is deduced by constraining total energy conservation and momentum conservation of a fluid column, and by using dimensional reasoning (see Appendix). This expression means that the rate of variation of the potential energy appears as the difference between the rate of work done by the wind induced Reynolds stress at the bottom of the upper mixed layer (parameterized by $\alpha \rho_2 A_{v1}/h_1 \mathbf{U}_w^2$), and the rate of kinetic energy production

$$\left(\frac{1}{2} \rho_2 \mathbf{u}_{-h}^2 \frac{dh_1}{dt}\right)$$

when the thickness of the upper layer increases as the result of entrainment. This last term is only a corrective term.

Eq. (IV) is the result of a direct calculation of the rate of potential energy variation of a water column between state (I) and state (III) (Fig. 2).

In expression (III) the wind induced horizontal bulk velocity $\mathbf{U}_w$ must be defined. A wind induced momentum equation taking into account the following assumptions is defined:

$\mathbf{U}_w$ ($U_{wx}$, $U_{wy}$) is defined as the difference between the total current and the tidal current, sum of the barotropic and baroclinic components in the upper mixed layer only;

$\mathbf{U}_1$ ($u_1$, $v_1$) remains governed by Eqs. (II2) and (II3).

The total current $\mathbf{U}_{(1)}$ is governed by the momentum equation of system (B) (with $i = 1$) in which a wind stress term $\tau_s/\rho_1 h_1$ is added on the right-hand side. Subtracting the barotropic and baroclinic tide momentum equations leads to an equation for wind induced current. This equation can be written in terms of flow components:

$$\begin{cases} \dfrac{dD_{wx}}{dt} + D_{wx}\dfrac{\partial}{\partial x}(U + u_1) - fD_{wy} = \dfrac{\tau_{Sx}}{\rho_1} - \mu D_{wx} \\ \dfrac{dD_{wy}}{dt} + D_{wy}\dfrac{\partial}{\partial x}(V + v_1) + fD_{wx} = \dfrac{\tau_{Sy}}{\rho_1} - \mu D_{wy} \end{cases} \tag{V}$$

with

$$\frac{d}{dt} = \frac{\partial}{\partial t} + (U + u_1 + U_{wx})\frac{\partial}{\partial x}$$

A drag force $-\mu\,\mathbf{D}_w$ is introduced on the right-hand side of equations ($V$) to damp wind induced inertial oscillations. Such a linear damping term has already been introduced in a slab model of mixed layer currents (Pollard and Millard, 1970). Comparisons between model simulations and measured mixed layer currents lead us to choose values of $\mu$ so that 2 days $< \mu^{-1} <$ 10 days (D'Asaro, 1985). Here we take $\mu = 4.10^{-6}\,\mathrm{s}^{-1}$.

It must be noted that this type of decomposition is rigorously justified only when the nonlinear terms can be neglected in the hydrodynamic equations. However this procedure has become common practice in nonlinear internal wave dynamics. To get Eqs. (V) we assume that the wind action does not directly modify the baroclinic tidal dynamics. The modifications of these dynamics are induced by mixing processes.

From (III) and (IV) we get the following entrainment rate relationship:

$$\frac{dh_1}{dt} = \frac{2\alpha\dfrac{A_{v1}}{h_1}\mathbf{U}_w^2}{\dfrac{1}{3}g'h_1\dfrac{3h_1 + 2d}{2h_1 + d} + \mathbf{u}_{-h}^2}$$

Where

$$g' = g\frac{\rho_2 - \rho_1}{\rho_2} \text{ (reduced gravity).}$$

A bulk Richardson number for this wind mixing process can be defined by:

$$R_{is} = \frac{dE_P}{\frac{1}{2}\rho_2 \mathbf{U}_w^2 dh_1}$$

with the expression (IV) one gets:

$$R_{is} = \frac{1}{3}g'\frac{h_1}{\mathbf{U}_w^2}\frac{3h_1 + 2d}{2h_1 + d}.$$

The expression of the entrainment velocity can then be written:

$$W_{e1} = \frac{dh_1}{dt} = 2\alpha\frac{A_{v1}}{h_1}\left(R_{is} + \frac{\mathbf{u}_{-h}^2}{\mathbf{U}_w^2}\right)^{-1}$$

$u_{-h}$ is here unknown and must be related to the bulk properties. Following the parameterization described in the Appendix, the expression of the entrainment rate is taken to be:

$$W_{e1} = 2\alpha\frac{A_{v_1}}{h_1}R_{is}^{-a} \tag{VI}$$

where $\alpha = 0.205$ and $a = 0.9$ are two constant dimensionless parameters. The values of these parameters have been determined by fitting the entrainment law (VI) to the experimental results of Kato and Phillips (1969).

*ii. Internal mixing*

The local Richardson number in the thermocline layer is defined by:

$$R_{it} = \frac{g\frac{\rho_2 - \rho_1}{\rho_2}d}{(\Delta\mathbf{U})^2} = \frac{g'd}{(\Delta\mathbf{U})^2}$$

where $\Delta\mathbf{U}$ is the current shear velocity:

$$\Delta\mathbf{U} = \mathbf{U}_{(1)} - \mathbf{U}_{(2)} = \mathbf{U}_1 + \mathbf{U}_w - \mathbf{U}_2.$$

Thorpe (1971) has shown experimentally that if $R_{it} < 1/4$ the system becomes unstable. Kelvin-Helmholtz instabilities appear then and turbulent mixing widens the thermocline layer. This broadening of the intermediate thermocline layer is consistent

with a transformation of kinetic energy into potential energy with some loss of energy due to dissipation. The result of the process is a transformation of the vertical structure (IV.1) into (IV.2) (Fig. 2). The thermocline widens in a symmetrical manner, as a result of internal energy conservation. This mixing energized by shear production has been described in detail by Thorpe (1977) and Sherman *et al.* (1978). Corcos and Sherman (1976) have analyzed shear instabilities and they concluded that the thickness of the thermocline layer after the mixing has subsided is given by:

$$d = 0.3(\Delta U)^2/g' \qquad \text{(VII)}$$

This criterion is based on a readjustment of the Richardson number to $R_{it} = 0.3$.

Such a mixing mechanism is consistent with the conservation of a vertical linear structure of density in the thermocline layer. This property, appears here as a hypothesis; however it has been verified by experimental observations in estuaries by Geyer and Smith (1987).

*iii. Bottom mixing effect*

The first mixing process described above leads to an increase of the upper mixed layer thickness only. The result of the second mixing mechanism is to widen the thermocline layer, and then to reduce the thickness of the upper and lower mixed layers.

The third mixing process which is considered now is similar in the bottom layer to the first one in the surface layer, the wind friction on the sea surface being replaced by the tidal friction on the ocean bottom.

To parameterize the effect of bottom friction on the thermocline an "equivalent" flow $\mathbf{D}_B$ is defined by the equation:

$$\frac{d\mathbf{D}_B}{dt} + f\mathbf{z}_o \wedge \mathbf{D}_B = \frac{\tau_B}{\rho_2} - \mu\mathbf{D}_B \qquad \text{(VIII)}$$

where $\tau_B = -C_B\,\mathbf{U}\,|\mathbf{U}|$ is the bottom tidal friction, $\mathbf{U}$ the barotropic tidal current and $C_B$ the bottom drag coefficient taken to be $C_B = 2{,}5\ 10^{-3}$.

In the same way as in the upper layer, a Richardson number associated with the bottom process is defined by:

$$R_{iB} = \frac{g'H_2}{3}\,\frac{[3H_2 + 2d]}{2H_2 + d}\Big/\left(\frac{\mathbf{D_B}}{H_2}\right)^2$$

where $H_2 = D - h_2$ is the bottom mixed layer thickness.

The entrainment velocity $W_{e2}$ is also defined by:

$$W_{e2} = -\frac{dh_2}{dt} = 2\alpha\,\frac{A_{v2}}{H_2}\,R_{iB}^{-a} \qquad \text{(IX)}$$

where $A_{v2} = \nu_{*2}^2/N/\sqrt{2}$ and $\nu_{*2}$ is the bottom friction velocity given by $\nu_{*2} = \sqrt{\tau_B/\rho_2}$.

Eq. (IX) shows that $W_{e2}$ is small when $R_{iB}$ is large. This arises in regions where the bottom mixed layer is thick and where tidal currents are weak. Therefore the entrainment rate $W_{e2}$ can modify the bottom layer in a significant way only in shelf break and continental shelf areas. However, over the shelf edge of the Celtic Sea, the water depth is close to $D = 180$ m, and the bottom layer will never by shallow enough to induce an important thermocline erosion according to the relationship (IX).

This mixing process is schematized by state (V) (Fig. 2) where the stratification (V1) becomes (V2) after the bottom mixing has subsided.

$W_{e2}$ can also be enhanced when the bottom mixed layer becomes shallower, as the result of a long term wind mixing action.

In the general case the local time variations of the depth of the thermocline boundaries and of the temperature of the upper and lower mixed layer, are the results of the three mixing mechanisms described above.

*b. Simulation of mixing processes—internal waves interaction.* In order to simulate the interaction between the above mentioned mixing processes and the internal wave field, the global set of hydrodynamic equations and the relations describing mixing must be integrated numerically. The procedure that has been followed is described in detail below.

The various scalar variables examined are:

- $h_1$, $h_2$ respectively the upper and lower level of the thermocline with respect to the sea surface;
- $T_1$, $T_2$ respectively the upper and lower mixed layer temperature;
- $u_1$, $v_1$, $u_2$, $v_2$ the components of the baroclinic tidal currents $\mathbf{U}_1$, $\mathbf{U}_2$ in the upper and lower mixed layer;
- $D_{wx}$, $D_{wy}$ the components of the wind induced bulk flow $\mathbf{D}_w$ in the upper layer defined by Eqs. (V); the corresponding bulk velocity is $\mathbf{U}_w = \mathbf{D}_w/h_1$ and its components $(U_{wx}, U_{wy})$;
- $D_{Bx}$, $D_{By}$ the components of the "equivalent" flow $\mathbf{D}_B$ associated with bottom tidal friction and defined by Eq. (VIII).

In the above notation it is assumed that the total current velocity in the upper and lower layers may be written respectively $\mathbf{U}_{(1)} = \mathbf{U} + \mathbf{U}_1 + \mathbf{U}_w$ and $\mathbf{U}_{(2)} = \mathbf{U} + \mathbf{U}_2$.

The flow $\mathbf{D}_B$ is only used in the calculation of the entrainment velocity $W_{e2}$ of water from the intermediate layer into the bottom layer.

Surface and thermocline elevation due to the barotropic tide are neglected in the expressions of $h_1$ and $h_2$ ($\xi/D \ll 1$) so that $h_1 \simeq H_1$ and $h_2 \simeq D - h_2$. The tidal current $\mathbf{U}$ (U, V) is unaffected by this process.

Assuming that each variable is known at times $t - \Delta t$ and $t$, its new value at time $t + \Delta t$ has to be determined.

A first evaluation at time $t + \Delta t$ is obtained from system (II) (for variables $h_1$, $u_1$, $v_1$, $h_2$, $u_2$, $v_2$), and Eqs. (V) and (VIII) (for flows $\mathbf{D}_w$ and $\mathbf{D}_B$ respectively).

Bulk temperatures in the upper and lower layer are respectively given by the following heat conservation equations:

$$\frac{\partial T_1}{\partial t} + (U + u_1 + U_{wx}) \frac{\partial T_1}{\partial x} = \frac{Q_s}{\rho_1 C_P h_1} \tag{X}$$

$$\frac{\partial T_2}{\partial t} + (U + u_2) \frac{\partial T_2}{\partial x} = 0 \tag{XI}$$

Where $Q_s$ represents the net surface heat flux, sum of the sensible, latent and radiative heat exchange across the ocean-atmosphere interface and $C_p$ the specific heat of seawater. $Q_s$ is assumed to be entirely absorbed in the upper mixed layer.

For example, let $h_2^*$ be the first evaluation of $h_2$ at time $t + \Delta t$; $h_2^*$ is given by the following approximation of Eq. (II4):

$$h_2^* = h_2(t - \Delta t) - 2\Delta t \left[ DU(t) \frac{\partial}{\partial x} \left( \frac{h_2(t)}{D} \right) + \frac{\partial}{\partial x} (h_1(t) u_1(t)) - \frac{\partial}{\partial x} \left[ (h_2(t) - h_1(t)) \frac{u_1(t) + u_2(t)}{2} \right] \right]$$

The first evaluation of the other variables of system (II), (i.e. $h_1$, $u_1$, $v_1$, $u_2$, $v_2$), at time $t + \Delta t$ is carried out in the same way giving: $h_1^*$, $u_1^*$, $v_1^*$, $u_2^*$, $v_2^*$. Finite difference approximations of equations (IX) and (X) lead to the first evaluation of the mixed layer temperatures at time $t + \Delta t$: $T_1^*$, $T_2^*$. Thus, these values result from advection and surface heat fluxes for $T_1$, and from advection alone for $T_2$.

As the flow $\mathbf{D}_w$ is known at time $t$, the Richardson number $R_{is}$, related to "surface effect" mixing may be defined. A second estimation $h_1^{**}$ of $h_1(t + \Delta t)$ is then obtained from time differencing of the entrainment rate relationship (VI):

$$h_1^{**} = h_1^* + \frac{2\alpha A_{v1}}{h_1^*} (R_{is})^{-a} \Delta t$$

Vertical fluxes between the upper mixed layer and the thermocline layer affect neither the internal energy nor the horizontal momentum in the whole two upper layers of thickness $h_2^*$. A second estimation of $T_1$, $u_1$, $v_1$ at time $t + \Delta t$ is thus obtained: $T_1^{**}$, $u_1^{**}$, $v_1^{**}$:

$$T_1^{**} = T_2^* + [T_1^* - T_2^*][h_1^* + h_2^*]/[h_1^{**} + h_2^*]$$

$u_1^{**}$ and $v_1^{**}$ may be put together under the following vectorial form:

$$\mathbf{U}_1^{**} = \mathbf{U}_1^{*} - [\mathbf{U}_1^{*} - \mathbf{U}_2^{*}][h_1^{**} - h_1^{*}]/[h_1^{**} + h_2^{*}]$$

This last expression shows that mixing leads to a decrease of the internal wave energy.

A same procedure leads to a second evaluation of the bottom mixed layer parameters modified according to bottom mixing effect.

Thus, time differencing of the expression (IX) leads to:

$$h_2^{**} = h_2^{*} - \frac{2\alpha A_{v2}}{(D - h_2^{*})} (R_{iB})^{-a} \Delta t$$

$T_2^{**}$ and $\mathbf{U}_2^{**}$ are given by:

$$T_2^{**} = T_1^{**} + [T_2^{*} - T_1^{**}][2D - h_1^{**} - h_2^{*}]/[2D - h_1^{**} - h_2^{**}]$$
$$\mathbf{U}_2^{**} = \mathbf{U}_2^{*} + [\mathbf{U}_2^{*} - \mathbf{U}_1^{**}][h_2^{**} - h_2^{*}]/[2D - h_1^{**} - h_2^{**}]$$

Knowledge of $h_1^{**}, h_2^{**}, T_1^{**}, T_2^{**}, \mathbf{U}_1^{**}, \mathbf{U}_2^{**}, \mathbf{U}_w(t + \Delta t)$ leads to the computation of the Richardson number in the thermocline layer:

$$R_{it} = \frac{g'[h_2^{**} - h_1^{**}]}{(\Delta \mathbf{U})^2}$$

with:

$$g' = g\,\alpha_T\,[T_1^{**} - T_2^{**}]$$
$$\Delta \mathbf{U} = \mathbf{U}_1^{**} + \mathbf{U}_w(t + \Delta t) - \mathbf{U}_2^{**}$$

For the sake of simplicity, let X denote one of the variables $h_1, u_1, v_1, T_1, h_2, u_2, v_2, T_2$. Two cases can arise:

$-R_{it} \geq 0.25$: no internal mixing occurs because of layer stability. Estimations $X^{**}$ are then the final values $X(t + \Delta t)$ of the above variables.

$-R_{it} < 0.25$: shear instabilities occur and internal mixing thickens the thermocline layer until $R_{it} = 0.3$. The thermocline thickness is then given by the relationship (VII) and the depths $h_1(t + \Delta t)$ and $h_2(t + \Delta t)$ becomes:

$$h_1(t + \Delta t) = \frac{1}{2}[h_1^{**} + h_2^{**}] - \frac{d}{2}$$

$$h_2(t + \Delta t) = \frac{1}{2}[h_1^{**} + h_2^{**}] + \frac{d}{2}$$

Symmetrical variations of $h_1$ and $h_2$ are consistent with internal energy and momentum conservation. Thus internal mixing affects neither $\mathbf{U}_i$ nor $T_i$ values and: $\mathbf{U}_i(t + \Delta t) = \mathbf{U}_i^{**}$, $T_i(t + \Delta t) = T_i^{**}$, $(i = 1 \text{ or } 2)$.

Each variable $X$ is now known at time $t + \Delta t$, and a new time step can start:

## 4. Numerical investigations

Four sets of results are presented below. The first simulation deals with the internal tide wave only, that is without wind stress and heat fluxes at the air-sea interface. The second one shows the results of the interaction between mixing and internal tides with wind but without heat fluxes at the ocean surface. In the third simulation, a diurnal heat flux is introduced in the model. These numerical investigations are carried out by using only one barotropic tidal component to force the model. The following numerical

values for fixed parameters are chosen:

$D_o = 4\,000$ m: water depth over the abyssal plain
$D_1 = 180$ m: water depth over the continental shelf
$L = 50$ km: width of the continental slope
$f = 10^{-4}\text{s}^{-1}$: Coriolis frequency
$\omega_{M_2} = 1.4\ 10^{-4}\text{s}^{-1}$: angular tidal frequency ($M_2$ component)
$\xi_{oM_2} = 1$ m: incident tidal wave amplitude ($M_2$ component)
$T_{1o} = 17°\text{C}$: initial upper layer temperature
$h_{1o} = 20$ m: initial upper layer thickness
$T_{2o} = 12°\text{C}$: initial bottom layer temperature
$d_o = h_{2o} - h_{1o} = 5$ m: initial thermocline layer thickness

The numerical results shown start from time $t_o = 193$ hrs. For $t < t_o$, the internal tide field is not yet well established in all the domain.

Values of $D_o$, $D_1$, $L$, $\xi_{oM_2}$ are chosen to closely approximate the actual conditions found in the Bay of Biscay and the Celtic Sea. Values of $T_{1o}$, $T_{2o}$, $h_{1o}$ and $d_o$ are also close to those that can be measured in these areas in summer.

Numerical runs carried out with other initial values of $T_{1o}$, $T_{2o}$, $h_{1o}$ and $d_o$ lead to the following comments near the shelf break:

— a lower initial temperature difference between the two mixed layers (i.e. a lower value of $g'$) induces a larger internal tide range near the edge and reduces the baroclinic wave length;

— a larger initial depth of the thermocline enhances the internal tide amplitude.

However in the shelf break area the general shape of the thermocline oscillation with respect to time is not very sensitive to the variation of these parameters.

It can also be noticed that a steepening of the continental shelf slope leads to a generation of baroclinic waves of larger amplitude. On the other hand the model response is sensitive to the amplitude of the barotropic forcing: the local internal tide amplitude and shape are highly modified through the $M_2-S_2$ tidal modulation. This appears in the results of the last numerical investigation (Fig. 9b and 10b).

The last set of results deals with the comparison between model and *Ondine* 85 data. In the numerical run, two monochromatic tidal waves ($M_2$, $S_2$) are introduced as forcing terms in the model. This allows a model response at spring and neap tides. Surface forcing is also introduced in the model by means of the measured wind speed and heat fluxes at the sea surface. The characteristics of the $S_2$ tidal component are:

$$\omega_{s_2} = 1.4510^{-4}\text{s}^{-1}\text{:angular tidal frequency}$$

$$\xi_{os_2} = 0.35\text{ m:incident tidal wave amplitude}$$

Initial values of the depth and the thickness of the thermocline are chosen to closely approximate those observed during the *Ondine* 85 experiment:

$$h_{10} = 40\text{ m}$$

$$d_o = 10\text{ m}$$

The other parameters have the above prescribed values.

*a. Internal tide wave.* Results of the hydrodynamic model are shown on Figure 3. Graphs a, b, c and d show the time evolution of the upper and lower boundary of the thermocline at four points located respectively on the continental shelf at 10 km from the shelf edge, at the shelf break, on the continental slope at 10 km from the edge, and on the abyssal plain at 150 km from the shelf break. These results can be compared to Pingree's observations on the continental shelf of the Bay of Biscay, near the shelf break (Pingree *et al.*, 1984). A good agreement between the model and the experiments can be noticed.

The thickness of the thermocline adjust itself to agree with the Richardson number requirement $R_{ii} > 1/4$. The results are sensitive to the choice of the initial thicknesses of the thermocline ($d_o$) and the upper layer ($h_{1o}$) and to the initial mixed layer temperature difference ($T_{1o} - T_{2o}$). For instance, when a narrower initial thermocline layer is chosen, larger shear induced turbulence will develop, leading to a thickening of the thermocline. On the other hand, when an initial lower bulk temperature difference ($T_{1o} - T_{2o}$) is chosen, larger amplitude internal tides are induced at the shelf break, leading also to an enhance of shear instabilities whose issue is again to thicken the thermocline. The internal tide range over the edge is also sensitive to the initial depth of the thermocline boundaries: it is found to increase with increasing values of these parameters.

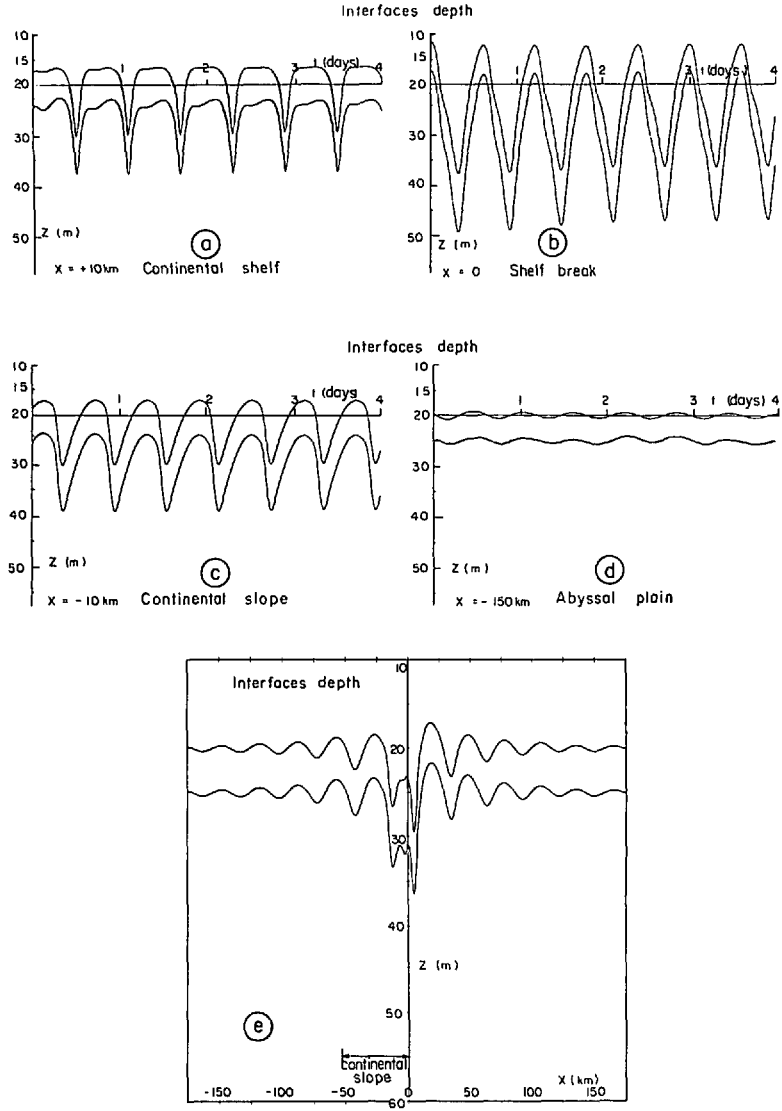


Figure 3. Temporal variations at four locations on the transect (a, b, c, d) and spatial variations at time $t = 289$ hrs of the depth of the upper and lower boundary of the thermocline (e).

Graph 3-e shows the shape of the interface, on the transect, at the end of the simulation ($t = 289$ hrs). The spatial variations of the depth of the thermocline boundaries are similar to the spatial oscillations of the interface depth in a two-layer ocean schematization described in a previous paper (Mazé, 1987).

*b. Interaction between internal waves and mixing processes without surface heat fluxes.* Figure 4 exhibits the model response to a sequence of two gusts of wind of sine

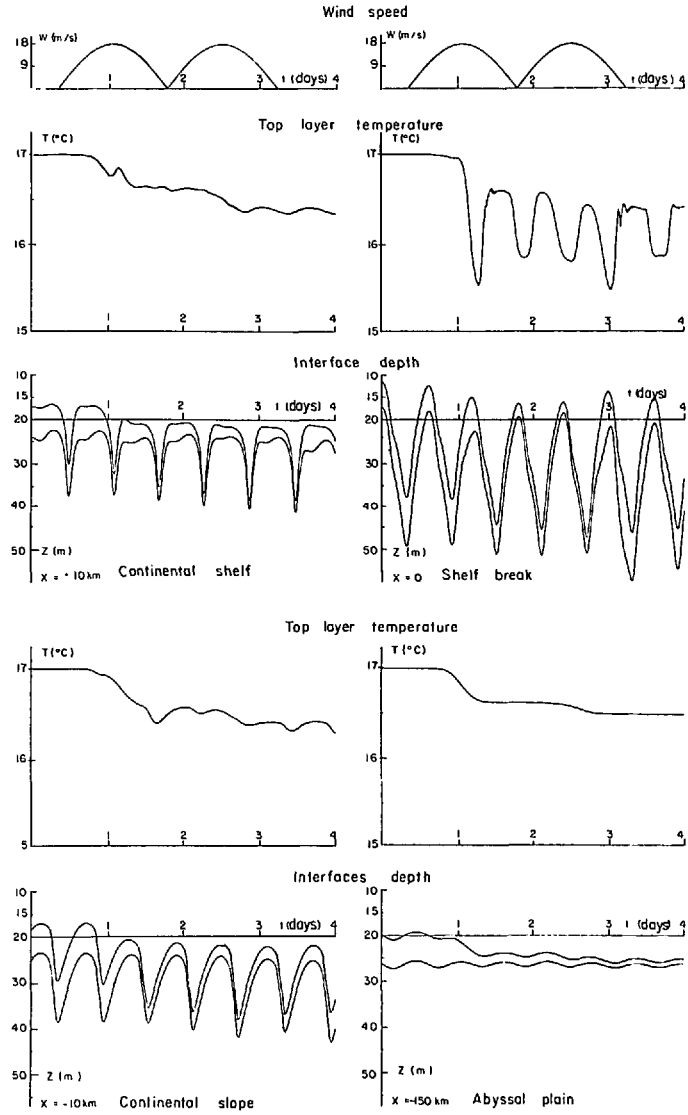


Figure 4. Interaction between internal tides and mixing: evolution with respect to time of the top layer temperature and interfaces depth at selected points on the transect.

shape. The wind speed amplitude is taken to be $W_o = 20$ m/s in the onshore direction (S-W wind in the Gulf of Biscay). Near the shelf break, the existence of large amplitude internal waves leads to important outcomes. Sea surface temperature takes a periodic character associated with advection and with spatial variation of mixing processes. Otherwise, in the shelf break area a decrease of the internal tide amplitude during the wind action can be noticed. Such an amplitude reduction is connected with momentum conservation whereas mixing proceeds, as it has been previously specified.

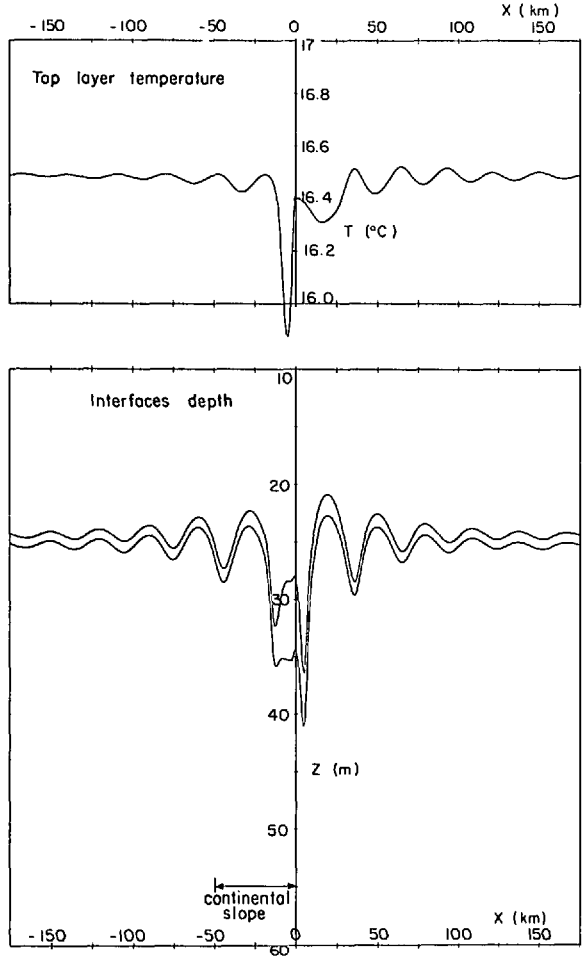


Figure 5. Interaction between internal waves and mixing: spatial variations of the top layer temperature and thermocline depth at time $t = 289$ hrs.

Furthermore, after the gust of wind has subsided, the internal wave amplitude increases as a result of proportionality between this amplitude and the upper mixed layer thickness. Moreover, the thermocline thickness variations appear clearly, as well as the deepening of the mean level of the thermocline.

The deepening and narrowing of the thermocline can be seen over the continental shelf and chiefly over the abyssal plain. This is the result of thermocline erosion due to wind, and shear instabilities. The thickness of the thermocline remains consistent with the Richardson number criterion $R_{ii} > 1/4$. After the end of wind action the wind induced current in the top layer decreases, shear instabilities disappear and then internal mixing vanishes.

Finally, Figure 5 shows the persistence of a colder surface water area over the shelf

break, with warmer water on the continental shelf and the abyssal plain. This "spot" of cold water is advected on both sides of the shelf break according to the current direction in the surface layer. The temperature difference between cold and warm water is close to 0.5°C. This result is compatible qualitatively with satellite infrared images on which a narrow ribbon of cool water, aligned with the top of the continental solpe, can often be observed in the north of the Bay of Biscay (Celtic shelf break) during summer and autumn (Pingree and Mardell, 1981; Mazé, 1983; Mazé *et al.*, 1986; Langlois *et al.*, 1990).

It is clear that this computed temperature difference between cold and warm water is sensitive to the initial values $T_{1o} - T_{2o}$, $h_{1o}$ chosen for this run. Thus, when lower values $T_{1o} - T_{2o}$ are selected, the vertical stability decreases, leading to an increase of both the internal tide range and the internal mixing. The upper mixed layer becomes therefore narrower when the internal wave is up leading to an increase of the wind induced entrainment and to a connected larger cooling in the surface mixed layer. On the other hand when larger values of $h_{1o}$ are chosen, a weaker cooling of the upper mixed layer is observed because the entrainment rates are lower, and also because the entrained cool water has to be mixed through a thicker upper layer, in average. The results of the calculation at the end of the wind action are practically unaffected by the choice of $d_o$. This is due to the adjustment of the thermocline thickness through the Richardson number requirement. If a thick thermocline layer is chosen initially, it narrows quickly after the beginning of a gust of wind until shear instabilities appear inducing internal mixing.

These results are practically insensitive to the wind direction.

*c. Interaction between internal waves, wind and surface heat fluxes.* With no heat flux at the sea surface, the global cooling of the upper layer over the transect as a whole, appears to be too large. In order to take into account heat exchange at the sea surface, a diurnal heat flux has been introduced in the model in the following way:

$$\begin{cases} Q_s = Q_o \sin \Omega t & \text{for} \quad 2n\pi < \Omega t < (2n+1)\pi \\ Q_s = 0 & \text{for} \quad (2n+1)\pi < \Omega t < 2(n+1)\pi \end{cases}$$

with $\Omega = 2\pi/24\ \text{hrs}^{-1}$ and $Q_o = 500\ \text{w/m}^2$.

The results of this simulation are shown on Figures 6 and 7. It can be noticed that, far from the shelf edge, the top mixed layer temperature remains practically constant. Other wind induced typical features, such as thermocline depth evolution with respect to time at various locations on the transect, do not exhibit noticeable differences (Fig. 6). It can also be pointed out that horizontal temperature gradients are almost the same, near the shelf break as without surface heat fluxes (Fig. 7).

*d. Comparison between model and Ondine 85 experiment.* One goal of the *Ondine* 85 experiment was to investigate the interaction between the internal tide field and sea

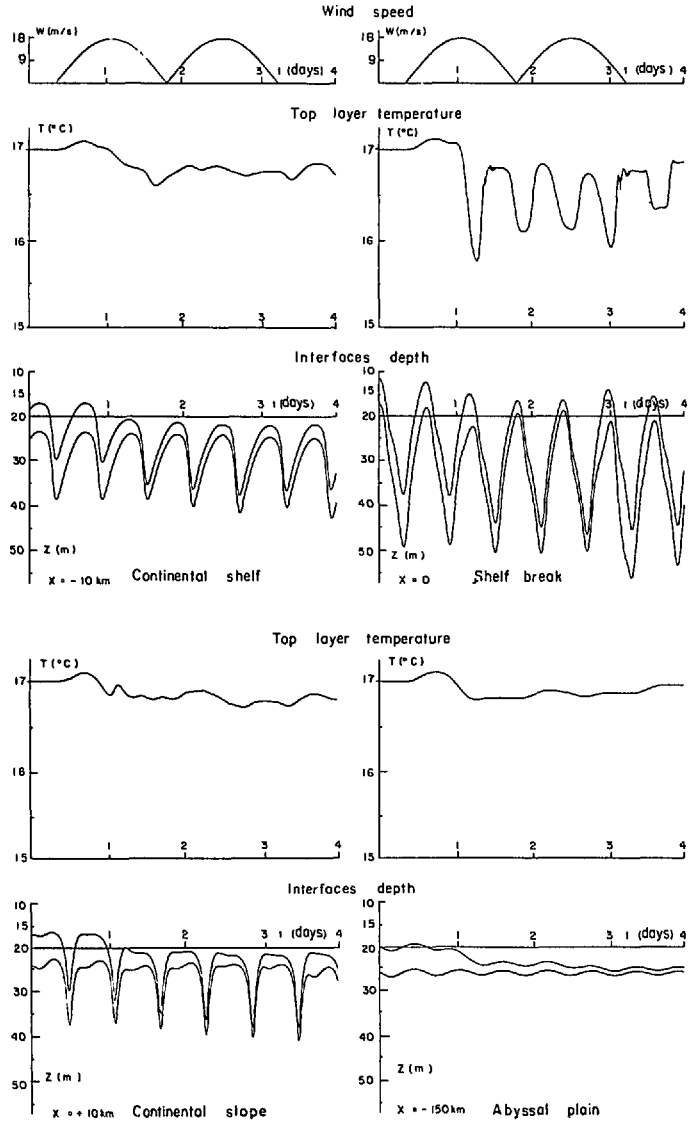


Figure 6. Interaction between internal waves, mixing and surface heat fluxes: evolution with respect to time (same as Fig. 4).

surface fluxes (heat flux, turbulent kinetic energy flux), in the shelf break area of the Celtic Sea. Toward that end, in late summer and early autumn 1985, two moorings with oceanographic instrumentation were deployed: $P_1$ located at the shelf break and $P_4$ on the shelf at 40 km from the edge (Fig. 8). Simultaneously, observations of the surface wind and the radiative budget were made, and the sensible and latent heat fluxes were evaluated from bulk formulae.

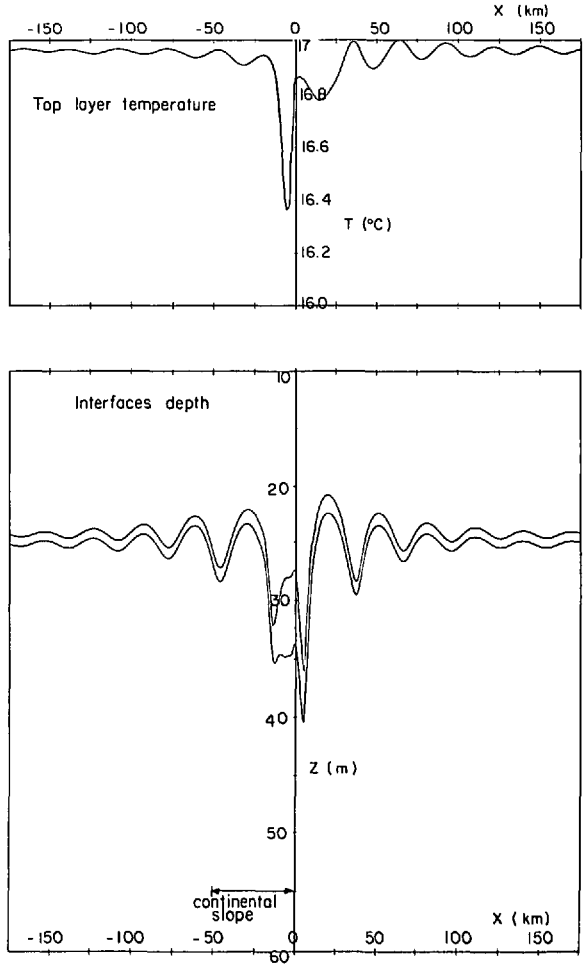


Figure 7. Interaction between internal waves, mixing and surface heat fluxes: spatial variations at time $t = 289$ hrs. (same as Fig. 5).

The moorings $P_1$ and $P_4$ provided the temperature data between 10 and 100 m depth. Measurements were taken by Aanderaa thermistor chains. The temperature observations were low-pass filtered in order to remove high frequency waves which are not of interest in the present study.

The isotherm depths where then computed as a function of time by interpolation between adjacent sensors.

The vertical displacements of the thermocline are shown by the time evolution of the depths of the isotherms 13.5°C and 15°C (Fig. 9a and 10a). The choice of these isotherms is due only to the fact that they remain in the range of depth of the records. The $M_2$ period and the $M_2 - S_2$ modulation appear clearly at moorings $P_1$ and $P_4$.

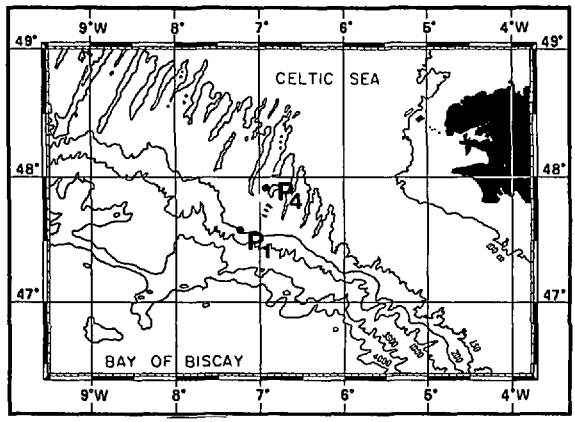


Figure 8. Location of moorings during *Ondine* 85 experiment.

A large portion of this tidal signal is due to the internal tide because larger displacements are absent in the barotropic tide. During a one week period (Sept. 30–Oct. 6) larger vertical displacements at tidal frequency are present at mooring $P_1$ than at mooring $P_4$, chiefly at spring tides (beginning of the period). This is consistent with the effectiveness of shelf break topography in generating internal tides from barotropic tides. These internal tides propagate onshelf and offshelf with a decay of their amplitude due to energy dissipation, as soon as they move away from the shelf break.

During the period studied, no gust of wind arose. The wind speed was close to 8–10 m/s in average. The heat budget at the sea surface was positive over a diurnal cycle.

A numerical experiment has been carried out with the following forcing terms:

— barotropic tidal forcing formed by two tidal components, $M_2$ and $S_2$, in order to reproduce spring and neap tides,

— wind forcing by the measured wind speed,

— heat fluxes computed from the measured radiative heat fluxes and the estimated sensible and latent heat fluxes.

The model response is shown at two points on the transect corresponding to the location of the moorings $P_1$ (Fig. 9b) and $P_4$ (Fig. 10b). The model gives results qualitatively in agreement with the data although the shape of the isotherms displacements deduced from the data exhibits a greater complexity than the thermocline depth evolution computed by the model. However we must remember some simplifications of the model: schematized bottom topography and vertical stratification, simplified

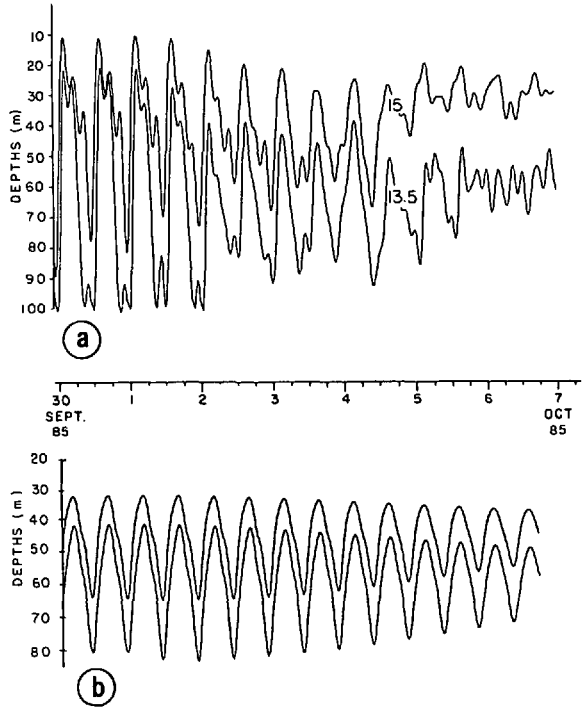


Figure 9. Time variation of the depth of: (a) Two isotherms in the thermocline deduced from data at location $P_1$. (b) The boundaries of the thermocline calculated by the model at the shelf break.

barotropic tide, alongshelf variations neglected. These simplifications allow the model to reproduce only the crude characteristics of the internal tide.

No significant deepening of the thermocline appears on Figures 9 and 10. Similarly the temperature data do not show a cooling of the top layer at spring tides. However, in the shelf break area, an entrainment rate may be expected at spring tide because of an increase of nutrients in the surface mixed layer during this period (P. Le Corre, private communication).

Winds blowing during the period under study were too weak to induce large entrainment of cool water in a rather thick surface mixed layer (40 m in average). On the other hand, a positive heat budget across the sea surface has been calculated. Therefore, it may be expected that during the period studied cooling due to wind induced entrainment has been balanced by warming due to a positive net heat flux across the sea surface.

Therefore, the *Ondine* 85 data are unfortunately not appropriate to test the cooling mechanism described in this study particularly because of too fair wind conditions during the experiment.

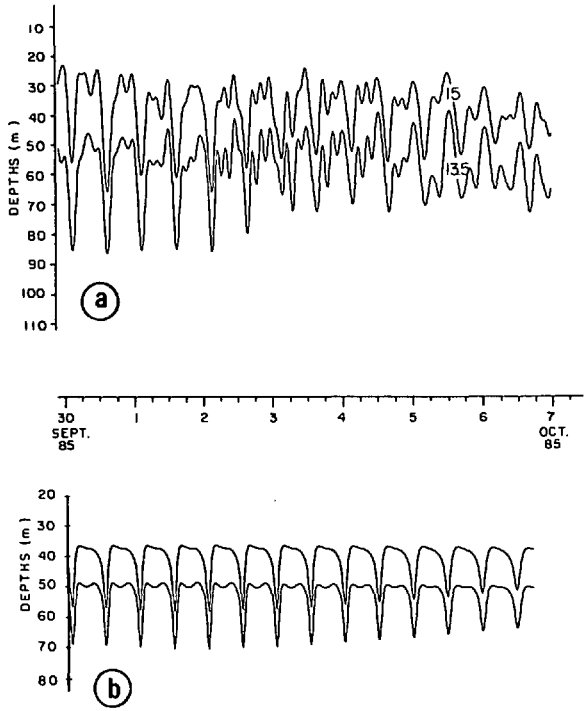


Figure 10. Time variation of the depth of: (a) Two isotherms in the thermocline deduced from data at location $P_4$. (b) The boundaries of the thermocline calculated by the model on the shelf at 40 km from the edge.

## 5. Conclusion

Our purpose, in the above study was to show that the interaction between internal tides and surface fluxes (wind, heat) is a process capable of creating a narrow ribbon of cool surface water centered over the shelf break. The model described here takes into account several mixing processes in the presence of internal tides over continental slope and shelf. Although simple, this model gives results which can be compared with experiments and satellite observations, in shelf break areas. In particular along the continental shelf edge of the Bay of Biscay, where the cooling increases in extent and intensity in a northwestward direction, it appears that intensification of cooling is in connection with the increase of barotropic, and associated baroclinic tidal currents. Thus in these areas where vertical shear is large even in the absence of a wind induced current in the top mixed layer, a gust of wind of a rather low intensity is able to produce entrainment of cool water from the lower layer into the surface layer just over the shelf break (this effect can be amplified if the wind blows during spring tides). Such a simulation may be done by introducing several monochromatic tidal waves (in particular the $M_2$ and $S_2$ components) as barotropic forcing of the model.

Use of a three-layer ocean model is here of a great interest in comparison with a two-layer one. Thus, comparison between numerical results and observations is better. Moreover, the three-layer scheme leads to a more realistic description of mixing processes.

The interaction between internal tides and energetic fluxes at the sea surface seems to be an attractive explanation of the celtic sea shelf break cooling.

Other explanations have been proposed to this characteristic of shelf break areas:

— Dickson *et al.* (1980) consider that shelf break cooling is the result of the interaction between Kelvin waves propagating along the continental slope and the slope topography.

— Heaps (1980) suggests that this phenomenon is due to an upwelling which appears along the shelf edge as the result of a cross-shelf wind action.

— New (1988) argues that cooling is due only to mixing created by internal motion that results from the interactions of the surface tide with bottom topography.

All these mechanisms may contribute to shelf break cooling. However, satellite imagery indicates that the shelf break cooling is larger in areas of strong tidal currents and therefore, of large internal tides amplitude and baroclinic currents. Shelf break cooling is also often enhanced at spring tides. Elsewhere it seems that the wind direction does not play an important role in the cooling process.

A recent analysis of infra-red images stemmed from Satellite NOAA has been carried out in the shelf break region of the Celtic Sea (Langlois *et al.*, 1990). The first two weeks of July 1987 were studied because of a persistent anticyclonic situation with weak winds (W $<$15 knots) during this period. The results show that shelf break cooling appears at spring tides in areas where the internal tide range is known to be large. Therefore it seems that weak winds blowing during a spring tide period suffice to induce shelf break cooling in these regions. The period analyzed in this study seems to be more favorable than late summer, to the observation of the phenomenon when anticyclonic conditions arise, because the surface layer is shallower in July than in September. These observations suggest that the mechanism described here is an active factor in the cooling process.

*Acknowledgments.* This research was carried out with the support of the French "Service Hydrographique et Océanographique de la Marine" (S.H.O.M.), of the "Direction des Recherches et Etudes Techniques" (D.R.E.T.), and of the "Institut National des Sciences de l'Univers" (I.N.S.U.).

Miss Christine Jacolot carefully typed the manuscript and Mr. Pierre Doaré drafted the figures.

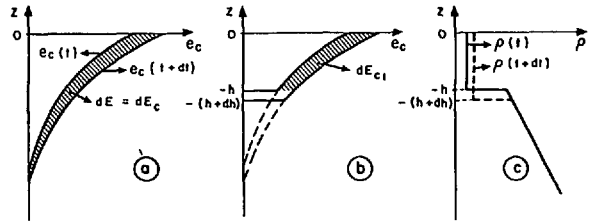


Figure 11. Diagrammatic representation of the time variation of: (a) The vertical structure of the kinetic energy in an homogeneous ocean. (b) The vertical structure of the kinetic energy in a stratified ocean. (c) The vertical structure of the density in a stratified ocean.

## APPENDIX

### Wind mixed layer deepening

A wind stress, acting over an ocean initially at rest creates turbulence and induces a current which decrease vertically from the surface. The total kinetic energy per unit volume $e_c$ is the sum of the turbulent kinetic energy $e_c^t$, and the kinetic energy of the mean motion $e_c^m$: $e_c = e_c^t + e_c^m$.

A schematic vertical structure of $e_c$ at times $t$ and $t + dt$ is shown on Figure 11a.

Assuming an adiabatic one dimensional process in a homogeneous ocean, the rate of variation of the total mechanical energy in a water column of unit section in the horizontal plane and of infinite depth may be written:

$$\frac{dE}{dt} = \int_{-\infty}^{0} \frac{de_c}{dt} = \frac{dE_c}{dt} = (\tau \cdot \mathbf{u})_o + F_o - \int_{-\infty}^{0} \epsilon \, dz \qquad (1)$$

Because of vertical homogeneity there is in this case no potential energy variation in the water column.

$(\tau \cdot \mathbf{u})_o$ is the rate of work of the wind stress $\tau$ on the sea surface, and $\mathbf{u}$ is the wind induced surface current;

$F_o$ is the turbulent kinetic energy flux across the sea surface;

$\epsilon$ is the rate of dissipation of turbulent kinetic energy by unit volume.

Consider now a stratified ocean which density structure is shown on Figure 11c (an upper mixed layer over a vertically stratified water) and the associate vertical structure of the kinetic energy (Fig. 11b). From time $t$ to time $t + dt$ the sharp thermocline deepens as the result of wind induced entrainment, and mixing of cold entrained water with warm water in the surface layer leads to an increase of the potential energy of the water column. The rate of variation of the mechanical energy of the whole water column is now:

$$\frac{dE}{dt} = \frac{dE_P}{dt} + \frac{dE_{c1}}{dt} + (e_c)_{-h} \frac{dh}{dt}$$

Where $dE_p/dt$ is the rate of variation of potential energy, $dE_{c1}/dt$ the rate of variation of kinetic energy in the mixed layer of thickness $h$, and $(e_c)_{-h}\, dh/dt$ the rate of variation of kinetic energy at the bottom of the mixed layer due to entrainment of quiescent water from below

$$(e_c)_{-h} = (e_c^t)_{-h} + \tfrac{1}{2}\rho \mathbf{u}^2_{-h}$$

where $\mathbf{u}_{-h}$ is the wind induced current velocity at the base of the mixed layer, and $\rho$ the density.

Assuming that $dE_{c1}/dt$ is the same as that in the case of a vertically homogeneous ocean, we may write:

$$\frac{dE_{c1}}{dt} = (\tau \cdot \mathbf{u})_o + F_o - (\tau \cdot \mathbf{u})_{-h} - F_{-h} - \int_{-h}^{0} \epsilon \, dz$$

where $(\tau \cdot \mathbf{u})_{-h}$ and $F_{-h}$ are respectively the rate of work of the Reynolds stress and the vertical flux of turbulent kinetic energy at depth $h$.

Therefore the rate of mechanical energy variation of the water column becomes:

$$\frac{dE}{dt} = \frac{dE_P}{dt} + (\tau \cdot \mathbf{u})_o + F_o - (\tau \cdot \mathbf{u})_{-h} - \int_{-h}^{0} \epsilon \, dz + \frac{1}{2}\rho \mathbf{u}^2_{-h} \frac{dh}{dt} \tag{2}$$

which takes into account the assumption of Niiler and Kraus (1977):

$$- F_{-h} + (e_c^t)_{-h} \frac{dh}{dt} = 0$$

The energy supplied to the ocean by the wind is transformed into kinetic energy in an homogeneous ocean and into kinetic and potential energy in a vertically stratified one.

From Eqs. (1) and (2) we get:

$$\frac{dE_P}{dt} = (\tau \cdot \mathbf{u})_{-h} - \frac{1}{2}\rho \mathbf{u}^2_{-h} \frac{dh}{dt} - \int_{-\infty}^{-h} \epsilon \, dz.$$

This equation means that the rate of variation of potential energy of a water column appears as equal to the rate of work of the Reynolds stress $\tau$ at the base of the mixed layer minus the rate of kinetic energy variation of the mean motion at this level due to entrainment minus the total rate of dissipation which would occur at depths greater than $h$ in a homogeneous water column. This last term is assumed to be small and will be neglected below. Therefore:

$$\frac{dE_P}{dt} = (\tau \cdot \mathbf{u})_{-h} - \frac{1}{2}\rho \mathbf{u}^2_{-h} \frac{dh}{dt}. \tag{3}$$

The rate of potential energy variation of a water column may be directly calculated when the vertical stratification is known.

In the case of a linearly stratified water column one gets:

$$\frac{dE_P}{dt} = \frac{1}{4}\rho N^2 h^2 \frac{dh}{dt} \tag{4}$$

where $N$ is the Brunt-Väisälä frequency.

Eqs. (3) and (4) lead to the following entrainment rate:

$$\frac{dh}{dt} = \frac{(\tau \cdot \mathbf{u})_{-h}}{\frac{1}{4}\rho N^2 h^2 + \frac{1}{2}\rho \mathbf{u}_{-h}^2} \tag{5}$$

$\mathbf{u}$ is given by the Ekman equation:

$$\frac{\partial \mathbf{u}}{\partial t} + f\mathbf{z}_o \wedge \mathbf{u} = \frac{\partial}{\partial z}\left(\frac{\tau}{\rho}\right) \tag{6}$$

where $f$ is the Coriolis frequency, $\tau = A_v\, \partial \mathbf{u}/\partial z$ and $A_v$ the vertical eddy viscosity coefficient.

The experimental results of Kato and Phillips (1969) in a nonrotating fluid are used to calibrate the model equations (5) and (6). Assuming a constant eddy viscosity in the whole mixed layer given by $A_v = v_*^2/N/\sqrt{2}$, where $v_*$ is the surface friction velocity, a good agreement with the above mentioned experiments is found.

Using dimensional reasoning, the term $(\tau \cdot \mathbf{u})_{-h}$ in (5) may be approximated by $\alpha\, \rho A_v/h\, U_w^2$. The entrainment law (5) is well parameterized by the relationship:

$$\frac{dh}{dt} = \alpha v_* \frac{A_v}{h} R_{iv}^{-a} \tag{7}$$

where

$$R_{iv} = \frac{dE_P}{\frac{1}{2}\rho U_w^2 dh}$$

is the bulk Richardson number of the mixed layer scaled by the vertically averaged wind induced velocity $U_w$, $\alpha$ and $a$ are two nondimensional constant parameters. The best agreement with the Kato-Phillip's data is obtained with $\alpha = 0.205$ and a $= 0.9$.

In a nonrotating fluid, the entrainment law (7) gives results quite close to those obtained using the slab models of Pollard, *et al.* (1973), and Price (1978).

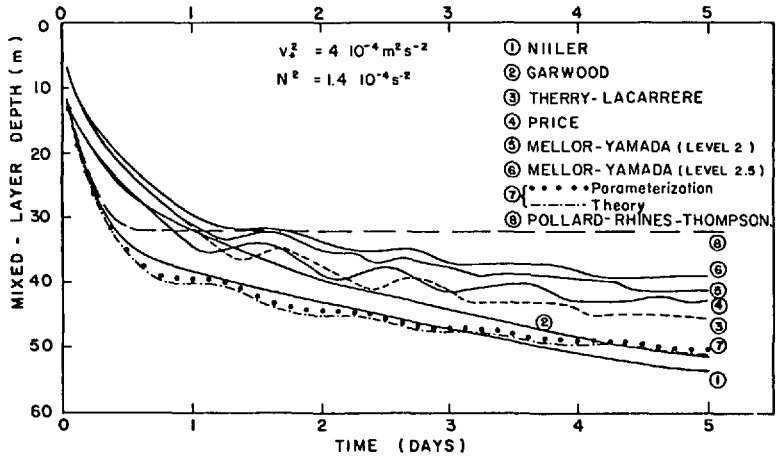


Figure 12. Comparison between various models of mixed layer deepening under the action of a constant wind stress on the surface of a rotating fluid linearly stratified initially (1 to 6 after Martin (1986)).

In a rotating environment the relationships (5) and (7) lead to thermocline deepenings larger than those given by the above-mentioned two models. A comparison with other slab models and models based on the turbulent kinetic energy budget has been carried out using the calculations of Martin (1986). The results shown on Figure 12 are obtained by forcing several models with a constant wind stress.

It must be noticed that in the study the hypothesis of a sharp thermocline is rather crude and that turbulence-internal wave processes near the base of the mixed layer are not taken here into account explicitely. However the Kelvin-Helmholtz instabilities are considered in an other way in the global model of interaction between internal tides and surface energetic fluxes.

## REFERENCES

Corcos, G. M. and F. S. Sherman. 1976. Vorticity concentrations and the dynamics of unstable shear layers. J. Fluid Mech., *73*, 241–264.

D'Asaro, E. A. 1985. The energy flux from the wind to near-inertial motion in the surface mixed layer. J. Phys. Oceanogr., *15*, 1043–1059.

Dickson, R. R., P. A. Gurbutt and N. V. Pillai. 1980. Satellite evidence of enhanced upwelling along the European Continental Shelf. J. Phys. Oceanogr., *10*, 813–819.

Geyer, W. R. and J. D. Smith. 1987. Shear instability in a highly stratified estuary. J. Phys. Oceanogr., *17*, 1668–1679.

Heaps, N. S. 1980. A mechanism for local upwelling along the European Continental Slope. Oceanol. Acta, *3*, 449–454.

Kato, H. and O. M. Phillips. 1969. On the penetration of a turbulent layer into a stratified fluid. J. Fluid Mech., *37*, 643–655.

Langlois, G., F. Gohin and A. Serpette. 1990. Refroidissements locaux aux abords du talus continental armoricain. Oceanol. Acta, *13*, 159–169.

Le Tareau, J. Y., R. Mazé, J. Le Fèvre, C. Billard and Y. Camus. 1983. ENVAT-81, Campagne de recherche multidisciplinaire en Atlantique: Aspects météorologiques, chimiques, biologiques, hydrologiques et thermodynamiques. Met-Mar, *118*, 6–25.

Martin, P. J. 1986. Testing comparison of several mixed-layer models. Naval Ocean Research and Development Activity, Report 143.

Mazé, R. 1983. Mouvements internes induits dans un golfe par le passage d'une dépression et par la marée. Thèse de Doctorat d'Etat, U.B.O., Brest.

——1987. Generation and propagation of non-linear internal waves induced by the tide over a continental slope. Cont. Shelf Res., *7*, 1079–1104.

Mazé, R., Y. Camus and J. Y. Le Tareau. 1986. Formation de gradients thermiques á la surface de l'Océan, au-dessus d'un talus, par interaction entre les ondes internes et le mélange dû au vent. J. Cons. Int. Explor. Mer, *42*, 221–240.

Mesinger, F. and A. Arakawa. 1976. Numerical Methods Used in Atmospheric Models. GARP Publications Series n. 17.

New, A. L. 1988. Internal tidal mixing in the Bay of Biscay. Deep-Sea Res., *35*, 691–709.

Niiler, P. P. and E. B. Kraus. 1977. One-dimensional models of the upper ocean, *in* Modeling and Prediction of the Upper Layers of the Ocean. E. B. Kraus ed., Pergamon Press, Oxford, 143–177.

Orlanski, I. 1976. A simple boundary condition for unbounded hyperbolic flows. J. Comp. Physics, *21*, 251–269.

Pichon, A. and R. Mazé. 1990. Internal tides over a shelf break. Analytical model and observations. J. Phys. Oceanogr. *20*, 657–671.

Pingree, R. D., D. K. Griffiths and G. T. Mardell. 1984. The structure of the internal tide at the Celtic Sea shelf break. J. Mar. Biol. Assoc. U.K., *64*, 99–113.

Pingree, R. D. and G. T. Mardell. 1981. Slope turbulence, internal waves and phytoplankton growth at the Celtic Sea shelf-break. Phil. Trans. R. Soc. Lond., *A 302*, 663–682.

Pollard, R. T. and R. C. Millard. 1970. Comparison between observed and simulated wind-generated inertial oscillations. Deep-Sea Res., *17*, 813–821.

Pollard, R. T., P. B. Rhines and R. O. R. Y. Thompson. 1973. The deepening of the wind mixed layer. Geophys. Fluid Dyn., *3*, 381–404.

Price, J. F. 1979. On the scaling of stress-driven entrainment experiments. J. Fluid Mech., *90*, 509–529.

Serpette, A. and R. Mazé. 1989. Internal tides in the Bay of Biscay: A two-dimensional model. Cont. Shelf Res., *9*, 795–821.

Sherman, F. S., J. Imberger and G. M. Corcos. 1978. Turbulence and mixing in stably stratified waters. Ann. Rev. Fluid Mech., *10*, 267–288.

Thorpe, S. A. 1971. Experiments on instability of stratified shear flows: Miscible fluids. J. Fluid Mech., *46*, 299–320.

——1977. Turbulence and mixing in a Scottish loch. Philos. Trans. R. Soc. London, *A 286*, 125–181.

Turner, J. S. 1981. Small-scale mixing processes, *in* Evolution of Physical Oceanography, B. A. Warren and C. Wunsch, eds., MIT Press, Cambridge, MA, 236–262.

Received: *16 March, 1989;* revised: *20 March, 1990.*